# A live-cell imaging system for visualizing the transport of Marburg virus nucleocapsid-like structures

Yuki Takamatsu[1, 3], Takeshi Noda[3,4*] and Stephan Becker[1,2*]

[1]Institut für Virologie, Philipps-Universität Marburg, Germany;

[2]German Center of Infection Research (DZIF), partner site Giessen-Marburg-Langen, Marburg, Germany;

[3]Laboratory of Ultrastructural Virology, Institute for Frontier Life and Medical Sciences, Kyoto University, Japan

[4]Laboratory of Ultrastructural Virology, Graduate School of Biostudies, Kyoto University, Japan

*Corresponding authors:

Takeshi Noda

Laboratory of Ultrastructural Virology

Institute for Frontier Life and Medical Sciences

Kyoto University

Japan

Tel.: +49 6421/28-66254

Fax.: +49 6421/28-68962

Email: t-noda@kyoto-uni.ac.jp

Stephan Becker

Institute of Virology

Philipps-University Marburg

Hans-Meerwein-Straße

35043 Marburg

Germany

Tel.: +49 6421/28-66254

Fax.: +49 6421/28-68962

Email: becker@staff.uni-marburg.de

**Abstract**

Live-cell imaging is a powerful tool for visualization of the spatio-temporal dynamics of living organisms. Although this technique is utilized to visualize nucleocapsid transport in Marburg virus (MARV)- or Ebola virus-infected cells, the experiments require biosafety level-4 (BSL-4) laboratories, which are restricted to trained and authorized individuals. To overcome this limitation, we developed a live-cell imaging system to visualize MARV nucleocapsid-like structures using fluorescence-conjugated viral proteins, which can be conducted outside BSL-4 laboratories. Our experiments revealed that nucleocapsid-like structures have similar transport characteristics to nucleocapsids observed in MARV-infected cells. This system provides a safe platform to evaluate antiviral drugs that inhibit MARV nucleocapsid transport.

46 **Introduction**

47 Marburg virus (MARV), together with the Ebola virus (EBOV), belongs to
48 the family *Filoviridae*, and has a roughly 19 kb non-segmented, single-stranded,
49 negative-sense RNA genome. It causes severe hemorrhagic fever with high
50 fatality rates. MARV epidemics have occasionally been reported in Central Africa,
51 with the largest one, having a 90% fatality rate, being reported in Angola between
52 2004 and 2005 (CDC, 2014). Currently, there are no approved vaccines or
53 antiviral therapeutics available to prevent or treat MARV infection. Therefore,
54 understanding the interplay between viral and host proteins during MARV
55 replication is necessary to establish countermeasures for the diseases. For
56 example, revealing the mechanisms for the assembly and transport of
57 nucleocapsids, which comprise viral genomic RNA, nucleoprotein (NP), viral
58 proteins (VP24, VP30, VP35), and polymerase L, and are responsible for the
59 transcription and replication of the viral genome, might contribute to the
60 development of new therapeutic options.

61 The main nucleocapsid protein of MARV is NP, which is responsible for
62 the encapsidation of single-stranded viral genomic RNA (Bharat *et al.*, 2012,
63 Muhlberger *et al.*, 1999). In addition to NP, MARV nucleocapsids also contain the

64 minor matrix protein VP24 and the polymerase cofactor VP35, both of which are
65 essential structural elements that directly interact with NP to build a helical
66 nucleocapsid approximately 1000 nm in length and 50 nm in diameter (Huang *et*
67 *al.*, 2002, Watanabe *et al.*, 2006, Bharat et al., 2012). Furthermore, the viral
68 polymerase L and the transcription factor VP30 are also associated with the
69 nucleocapsid (Hartlieb *et al.*, 2003, Biedenkopf *et al.*, 2013). The core complex
70 of the nucleocapsid, formed by the NP, VP35, and VP24 proteins together with
71 the viral RNA, is defined as a nucleocapsid-like structure (NCLS, Fig. 1a). In
72 MARV- and EBOV-infected cells, immunofluorescence microscopy, as well as
73 live-cell imaging, have been used to visualize and analyze nucleocapsids by
74 fluorescently labeling the nucleocapsid proteins (Schudt *et al.*, 2013, Schudt *et*
75 *al.*, 2015, Becker *et al.*, 1996, Kolesnikova *et al.*, 2004a, Kolesnikova *et al.*,
76 2004b). According to these reports, nucleocapsid formation occurs in the
77 perinuclear inclusion bodies, following which they are transported into the
78 cytoplasm and redistributed prior to budding through the cell surface. The velocity
79 of nucleocapsid movement inside cells ranges from 100 nm/s to 500 nm/s in
80 MARV- or EBOV-infection (Schudt et al., 2013, Schudt et al., 2015). Application
81 of specific cytoskeleton inhibitors revealed that the transport of MARV

82 nucleocapsids was dependent on actin polymerization. Viral matrix protein VP40,
83 which is a peripheral membrane protein and plays a pivotal role in filamentous
84 virion formation, is essential for the recruitment of nucleocapsids to the cell
85 periphery and for their incorporation into progeny virions (Noda *et al.*, 2007,
86 Bharat et al., 2012, Noda *et al.*, 2002, Dolnik *et al.*, 2010). The surface
87 glycoprotein GP, which is an integral membrane protein and is responsible for cell
88 entry, forms the filamentous virions together with VP40 (Fig. 1b) (Becker et al.,
89 1996, Mittler *et al.*, 2007, Beniac & Booth, 2017, Booth *et al.*, 2013).

90 Live-cell imaging is a powerful tool for visualization of the spatio-temporal
91 dynamics of living organisms. In addition to immunofluorescence microscopy,
92 live-cell imaging microscopy has been utilized to visualize the localization of viral
93 proteins, and interactions between viral and host proteins in various virus-infected
94 cells (Nanbo *et al.*, 2013, Hoenen *et al.*, 2012, Lakdawala *et al.*, 2014, Becker et
95 al., 1996). However, because of its high pathogenicity, MARV must be handled
96 under the highest biosafety conditions [biosafety level 4 (BSL-4)], which
97 complicates and delays research using live-cell imaging (Falzarano *et al.*, 2011).
98 In this study, we developed a safe, live-cell imaging system, following a previously
99 established method for EBOV (Takamatsu *et al.*, 2018), to visualize MARV

100 nucleocapsid-like structures (NCLSs) in cells expressing viral proteins, outside of
101 BSL-4 laboratories. By using this live-cell imaging system, we were able to
102 analyze interactions between NCLSs and the cellular cytoskeleton, as well as
103 intracellular transport of NCLSs.
104
105

106 **Materials and methods**

107 **Cell culture.**

108 Huh-7 (human hepatoma) cells were maintained at 37 °C and 5% $CO_2$ in
109 Dulbecco's Modified Eagle Medium (DMEM, Life Technologies) supplemented
110 with 10% (vol/vol) Fetal bovine serum (FBS , PAN Biotech), 5 mM L-glutamine
111 (Q; Life Technologies), 50 U/mL penicillin, and 50 µg/mL streptomycin (PS; Life
112 Technologies).

113

114 **Plasmids and transfection.**

115 Plasmids encoding the MARV structural proteins (NP, VP35, VP24, L, VP40 and
116 GP): pCAGGS-NP, pCAGGS-VP35, pCAGGS-VP24, pCAGGS-L, pCAGGS-
117 VP40, and pCAGGS-GP, and a MARV minigenome-expressing plasmid which
118 encodes a *Renilla* luciferase were used (Wenigenrath *et al.*, 2010, Hoenen *et al.*,
119 2011). The plasmid pCAGGS-VP30-GFP, coding for the green fluorescent
120 protein-VP30 fusion protein, was produced as previously described (Schudt et al.,
121 2013). The transfection was performed in 50 µL Opti-MEM without phenol red
122 (Life Technologies) using TranSIT (Mirus) according to the manufacturer's
123 instructions.

124

125 **Lice cell imaging microscopy.**

126 A total of $2\times10^4$ Huh-7 cells were seeded onto a μ-Slide 4 well (Ibidi) and
127 cultivated in DMEM/PS/Q with 10% FBS. Each well was transfected with the
128 following plasmids, encoding all MARV structural proteins: (250 ng of pCAGGS-
129 NP, 50 ng of pCAGGS-VP35, 125 ng of pCAGGS-VP30-GFP, 50 ng of pCAGGS-
130 VP24, 500 ng of pCAGGS-L, 125 ng of pCAGGS-VP40 and 125 ng of pCAGGS-
131 GP), together with a T7-driven, MARV minigenome-expressing plasmid, which
132 encodes a *Renilla* luciferase, and a T7 polymerase-coding plasmid (pCAGGS-
133 T7) (Wenigenrath et al., 2010, Hoenen et al., 2011). The inoculum was removed
134 at 1 h post-transfection (p.t.), and 500 μL $CO_2$-independent Leibovitz's medium
135 (Life Technologies) with PS/Q, non-essential amino acid solution, and 20%
136 (vol/vol) FBS were added. Live-cell time-lapse experiments were recorded with a
137 Nikon ECLIPSE TE2000-E using a 63× oil objective or a GE healthcare Delta
138 Vision Elite using a 60× oil objective in biosafety level-2 laboratories.

139

140 **Treatment of cells with cytoskeleton-modulating drugs.**

141 Cells were treated with 15 μM nocodazole (Sigma), 0.3 μM cytochalasin D

142 (Sigma), or 0.15% dimethyl sulfoxide (DMSO, Sigma), following previous
143 publication (Schudt et al., 2013). The chemicals were added to the cell culture
144 medium 3 hours prior to observation.
145
146 **Image processing and analysis.**
147 Acquired pictures and movie sequences were processed using the Fiji plugin
148 “TrackMate” (Tinevez *et al.*, 2017, Schindelin *et al.*, 2012).
149

## Results and Discussion

### Establishment of a live-cell imaging system for MARV NCLSs transport.

The Marburg virus VLP system, which models a complete, single infectious cycle, has been developed and used to analyze transcription and replication, as well as the budding processes (Wenigenrath et al., 2010, Hoenen et al., 2011). In this study, we attempted to visualize MARV NCLSs transport in Huh-7 cells, which is a suitable method to determine the sequential intracytoplasmic movement of MARV nucleocapsids (Schudt et al., 2013), by using this VLP system following the procedure established in EBOV (Takamatsu et al., 2018). Transfection of the VLP components with the following modifications: replacing VP30 with VP30-GFP, was performed as described in Figure 2a. We employed this VLP-based system in all subsequent experiments in this study.

At 18 h p.t., we detected a large number of signals with various shapes (Supplementary Movie 1). Over 1,000 signals in the acquired movie sequences were analyzed. The representing sequence was expressed as the maximum intensity projection, in which the image projected maximum intensity of each time-lapse were plotted. (Fig. 2b). Among the signals, we focused on the signals

168 showing long-distance and directional transport, which represent NCLSs
169 trajectories (Takamatsu et al., 2018). We detected trajectories with lengths
170 ranging from 100 nm to 20 μm, with a mean length of 1.89 ± 0.91 μm (Fig. 2c).
171 The direction of movement of each NCLS also varied, though the cause of this
172 variation remains unclear. The speed of MARV NCLSs transport ranged from 10
173 nm/s to 500 nm/s, with a mean velocity of 167 ± 96 nm/s (Fig. 2d), which is
174 comparable to the velocity of nucleocapsids transport in MARV-infected cells
175 analyzed in BSL-4 laboratories (Schudt et al., 2013). In summary, the movement
176 characteristics of NCLSs in our system is similar to those of nucleocapsids in
177 MARV-infected cells.

178 **Actin polymerization is required for MARV NCLSs transport.**

179 In MARV-infected cells, the microtubule depolymerizing drug nocodazole
180 does not alter the movement of nucleocapsids, whereas the actin depolymerizing
181 drug cytochalasin D arrests it (Schudt et al., 2013). To confirm the relevance of
182 the live-cell imaging system we developed in this study, we analyzed NCLSs
183 movement after treatment with cytoskeletal modulation drugs. Huh-7 cells were
184 transfected with plasmids as described in Figure 2a. The culture medium was
185 replaced at 15 h p.t. with Leibovitz's medium containing either 0.15 % DMSO

186 (control), 0.15 M nocodazole, or 0.3 μM cytochalasin D (Fig. 3a-d, Supplementary
187 Movie 2-4) (Schudt et al., 2013). After incubation the cells with cytoskeletal
188 modulating drugs for 3h, time-lapse images were acquired. Nocodazole
189 treatment did not alter the trajectory length of NCLSs transport in comparison to
190 the control, whereas cytochalasin D treatment induced immediate cessation of
191 long-distance transport (Fig. 3e-g). The mean velocity of NCLSs transport in the
192 control or nocodazole-treated cells was 188 ± 98 nm/s and 219 ± 99 nm/s,
193 respectively (Fig. 3h). On the other hand, only a few non-specific NCLSs
194 movements were detectable in cytochalasin D-treated cells, with a mean velocity
195 of 2.73 ± 23 nm/s (Fig. 3i-j). These results confirmed that NCLSs transport is
196 dependent on actin polymerization, as well as the availability of our assay to test
197 candidate drugs which target nucleocapsid intracellular transport.
198

199 **Concluding remarks**

200 In the present study, we developed a live-cell imaging system for cells
201 expressing viral proteins, which can be safely used in BSL-2 laboratories.
202 Furthermore, we demonstrated the relevance of our system as a substitute for
203 the analysis of nucleocapsids transport in MARV-infected cells. Currently, cellular

factors involved in the nucleocapsid transport have not been fully understood. The combined approach of gene silencing and inhibitor screening using the system we developed can be utilized to identify the key host factors for the intracellular transport of MARV nucleocapsids. Moreover, it is noteworthy that the technical approach developed here might be applicable to study the nucleocapsid transport of other mononegaviruses, as well as to characterize antivirals inhibiting nucleocapsid transport.

**Acknowledgments**

The authors are grateful to Olga Dolnik and Gordian Schudt (Philipps University Marburg, Germany) for fruitful discussion.

**Funding**

The work was supported by Japan Society for the Promotion of Science JSPS Grant number 18J01631, 19K16666 (to Y.T.), by AMED, Research Program on Emerging and Re-emerging Infectious Diseases, by AMED Japanese Initiative for Progress of Research on Infectious Disease for global Epidemic, by JSPS Core-to-Core Program A, the Advanced Research Networks, by Grant for Joint Research Project of the Institute of Medical Science, University of Tokyo, by Joint Usage/Research Center program of Institute for Frontier Life and Medical Sciences Kyoto University, by the Daiichi Sankyo Foundation of Life Science, and by the Takeda Science Foundation (to T.N.), and by the Deutsche Forschungsgemeinschaft (DFG, German research foundation) Project number 197785619-SFB 1021 (to S.B.).

## References


Becker, S., Klenk, H. D. & Muhlberger, E. (1996) Intracellular transport and processing of the Marburg virus surface protein in vertebrate and insect cells. *Virology,* 225, 145-155.

Beniac, D. R. & Booth, T. F. (2017) Structure of the Ebola virus glycoprotein spike within the virion envelope at 11 A resolution. *Scientific reports,* 7, 46374.

Bharat, T. A., Noda, T., Riches, J. D., Kraehling, V., Kolesnikova, L., Becker, S., Kawaoka, Y. & Briggs, J. A. (2012) Structural dissection of Ebola virus and its assembly determinants using cryo-electron tomography. *Proceedings of the National Academy of Sciences of the United States of America,* 109, 4275-4280.

Biedenkopf, N., Hartlieb, B., Hoenen, T. & Becker, S. (2013) Phosphorylation of Ebola virus VP30 influences the composition of the viral nucleocapsid complex: impact on viral transcription and replication. *The Journal of biological chemistry,* 288, 11165-11174.

Booth, T. F., Rabb, M. J. & Beniac, D. R. (2013) How do filovirus filaments bend without breaking? *Trends in microbiology,* 21, 583-593.

CDC (2014) Chronology of Marburg Hemorrhagic Fever Outbreaks.

Dolnik, O., Kolesnikova, L., Stevermann, L. & Becker, S. (2010) Tsg101 is recruited by a late domain of the nucleocapsid protein to support budding of Marburg virus-like particles. *Journal of virology,* 84, 7847-7856.

Falzarano, D., Geisbert, T. W. & Feldmann, H. (2011) Progress in filovirus vaccine development: evaluating the potential for clinical use. *Expert review of vaccines,* 10, 63-77.

Hartlieb, B., Modrof, J., Muhlberger, E., Klenk, H. D. & Becker, S. (2003) Oligomerization of Ebola virus VP30 is essential for viral transcription and can be inhibited by a synthetic peptide. *The Journal of biological chemistry,* 278, 41830-41836.

Hoenen, T., Groseth, A., de Kok-Mercado, F., Kuhn, J. H. & Wahl-Jensen, V. (2011) Minigenomes, transcription and replication competent virus-like particles and beyond: reverse genetics systems for filoviruses and other negative stranded hemorrhagic fever viruses. *Antiviral research,* 91, 195-208.

Hoenen, T., Shabman, R. S., Groseth, A., Herwig, A., Weber, M., Schudt, G., Dolnik, O., Basler, C. F., Becker, S. & Feldmann, H. (2012) Inclusion bodies are a site of ebolavirus replication. *Journal of virology,* 86, 11779-11788.

Huang, Y., Xu, L., Sun, Y. & Nabel, G. J. (2002) The assembly of Ebola virus nucleocapsid requires virion-associated proteins 35 and 24 and posttranslational modification of nucleoprotein. *Molecular cell,* 10, 307-316.

265 Kolesnikova, L., Bamberg, S., Berghofer, B. & Becker, S. (2004a) The matrix protein of
266 Marburg virus is transported to the plasma membrane along cellular membranes:
267 exploiting the retrograde late endosomal pathway. *Journal of virology,* 78, 2382-2393.
268 Kolesnikova, L., Berghofer, B., Bamberg, S. & Becker, S. (2004b) Multivesicular bodies as a
269 platform for formation of the Marburg virus envelope. *Journal of virology,* 78, 12277-
270 12287.
271 Lakdawala, S. S., Wu, Y., Wawrzusin, P., Kabat, J., Broadbent, A. J., Lamirande, E. W., Fodor,
272 E., Altan-Bonnet, N., Shroff, H. & Subbarao, K. (2014) Influenza a virus assembly
273 intermediates fuse in the cytoplasm. *PLoS pathogens,* 10, e1003971.
274 Mittler, E., Kolesnikova, L., Strecker, T., Garten, W. & Becker, S. (2007) Role of the
275 transmembrane domain of marburg virus surface protein GP in assembly of the viral
276 envelope. *Journal of virology,* 81, 3942-3948.
277 Muhlberger, E., Weik, M., Volchkov, V. E., Klenk, H. D. & Becker, S. (1999) Comparison of
278 the transcription and replication strategies of marburg virus and Ebola virus by
279 using artificial replication systems. *Journal of virology,* 73, 2333-2342.
280 Nanbo, A., Watanabe, S., Halfmann, P. & Kawaoka, Y. (2013) The spatio-temporal
281 distribution dynamics of Ebola virus proteins and RNA in infected cells. *Scientific*
282 *reports,* 3, 1206.
283 Noda, T., Sagara, H., Suzuki, E., Takada, A., Kida, H. & Kawaoka, Y. (2002) Ebola virus VP40
284 drives the formation of virus-like filamentous particles along with GP. *Journal of*
285 *virology,* 76, 4855-4865.
286 Noda, T., Watanabe, S., Sagara, H. & Kawaoka, Y. (2007) Mapping of the VP40-binding
287 regions of the nucleoprotein of Ebola virus. *Journal of virology,* 81, 3554-3562.
288 Schindelin, J., Arganda-Carreras, I., Frise, E., Kaynig, V., Longair, M., Pietzsch, T., Preibisch,
289 S., Rueden, C., Saalfeld, S., Schmid, B., Tinevez, J. Y., White, D. J., Hartenstein, V.,
290 Eliceiri, K., Tomancak, P. & Cardona, A. (2012) Fiji: an open-source platform for
291 biological-image analysis. *Nature methods,* 9, 676-682.
292 Schudt, G., Dolnik, O., Kolesnikova, L., Biedenkopf, N., Herwig, A. & Becker, S. (2015)
293 Transport of Ebolavirus Nucleocapsids Is Dependent on Actin Polymerization: Live-
294 Cell Imaging Analysis of Ebolavirus-Infected Cells. *The Journal of infectious diseases,*
295 212 Suppl 2, S160-166.
296 Schudt, G., Kolesnikova, L., Dolnik, O., Sodeik, B. & Becker, S. (2013) Live-cell imaging of
297 Marburg virus-infected cells uncovers actin-dependent transport of nucleocapsids
298 over long distances. *Proceedings of the National Academy of Sciences of the United*
299 *States of America,* 110, 14402-14407.
300 Takamatsu, Y., Kolesnikova, L. & Becker, S. (2018) Ebola virus proteins NP, VP35, and VP24

are essential and sufficient to mediate nucleocapsid transport. *Proceedings of the National Academy of Sciences of the United States of America,* 115, 1075-1080.

Tinevez, J. Y., Perry, N., Schindelin, J., Hoopes, G. M., Reynolds, G. D., Laplantine, E., Bednarek, S. Y., Shorte, S. L. & Eliceiri, K. W. (2017) TrackMate: An open and extensible platform for single-particle tracking. *Methods,* 115, 80-90.

Watanabe, S., Noda, T. & Kawaoka, Y. (2006) Functional mapping of the nucleoprotein of Ebola virus. *Journal of virology,* 80, 3743-3751.

Wenigenrath, J., Kolesnikova, L., Hoenen, T., Mittler, E. & Becker, S. (2010) Establishment and application of an infectious virus-like particle system for Marburg virus. *The Journal of general virology,* 91, 1325-1334.

314 **Figure legends**

315 **Figure 1. Orientation of MARV nucleocapsid and its transport pathway.** (a)
316 The viral genome is encapsidated by NP. Nucleocapsids additionally contain
317 VP24, VP30, VP35, and L. Among them, NP, VP24, and V35 form the core
318 structure of the nucleocapsid called a “nucleocapsid-like structure (NCLS)”. (b)
319 Nucleocapsids are formed in the perinuclear inclusion bodies and are
320 subsequently transported along polymerized actin filaments to the plasma
321 membrane, where budding and release of virions takes place. The VP40 protein
322 forms filamentous virions together with GP.

323 **Figure 2. Live-cell imaging system of MARV nucleocapsid-like structures.**
324 (a) The experimental setting for detection of NCLS transport. Huh-7 cells were
325 transfected with plasmids encoding NP, L, VP35, VP24, VP40, GP, Marburg virus
326 specific minigenome, T7 polymerase, and VP30-GFP. (b) Plasmid-transfected
327 Huh-7 cells were observed at 18 h p.t. The image shows the maximum-intensity
328 projection of time-lapse images of cells, recorded for 90 seconds; images were
329 captured every 2 s. (c, d) Over 100,000 moving signals were captured and over
330 1,000 selected signals were analyzed using the Fiji plugin “TrackMate”. (c) The
331 length of the NCLS trajectories was evaluated. The y-axis represents the number

332 of signals in each range (x-axis). The numbers indicate mean ± SD (μm). (d) The
333 velocity of NCLSs transport was evaluated. The y-axis represents the number of
334 signals in each range (x-axis). The numbers indicate mean ± SD (nm/s).

335 **Figure 3. Effect of cytoskeleton-modulating drugs on MARV NCLSs**
336 **transport.** (a) Experimental setting to observe the effects of cytoskeleton
337 modulating drugs on MARV NCLSs transport. Huh-7 cells were transfected with
338 plasmids as described in Fig. 2(a), and treated at 15 h p.t. with either 0.15 %
339 DMSO (control), 0.15 μM nocodazole, or 0.3 μM cytochalasin D. After 3 hours of
340 treatment, observation of the cells began (18 h p.t.). (b-d) Time-lapse images
341 were acquired for each of the drug treated cells (b: DMSO, c: Nocodazole, d:
342 Cytochalasin D). The pictures show the maximum-intensity projection of time-
343 lapse images of cells, recorded for 90 seconds; images were captured every 2 s.
344 (e-i) Over 100,000 moving signals were captured and over 1,000 selected signals
345 were analyzed using Fiji plugin "TrackMate". (e-g) The length of the NCLS
346 trajectories was evaluated in each of the drug treated cells (e: DMSO, f:
347 Nocodazole, g: Cytochalasin D). The y-axis represents the number of signals in
348 each range (x-axis). The numbers indicate mean ± SD (μm). (h-i) The velocity of
349 NCLSs transport was evaluated in each of the drug treated cells (h: DMSO, i:

350 Nocodazole, j: Cytochalasin D). The y-axis represents the number of signals in

351 each range (x-axis). The numbers indicate mean ± SD (nm/s).

(a)

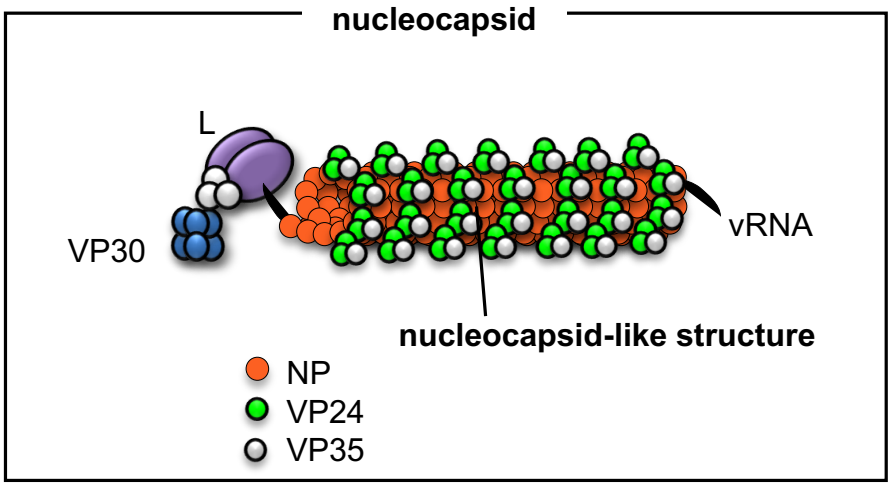
nucleocapsid
L
VP30
vRNA
nucleocapsid-like structure
NP
VP24
VP35

(b)

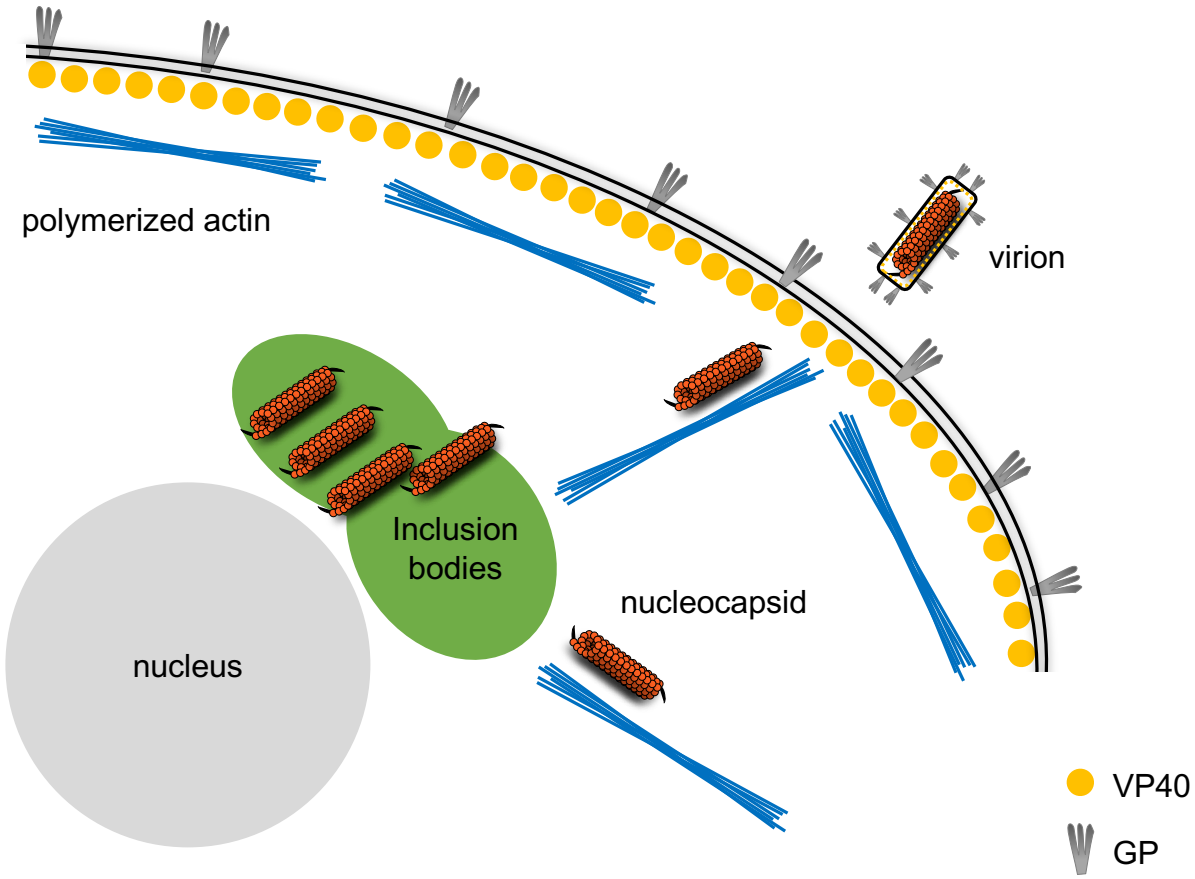
polymerized actin
virion
Inclusion bodies
nucleocapsid
nucleus
VP40
GP

**Figure 1**

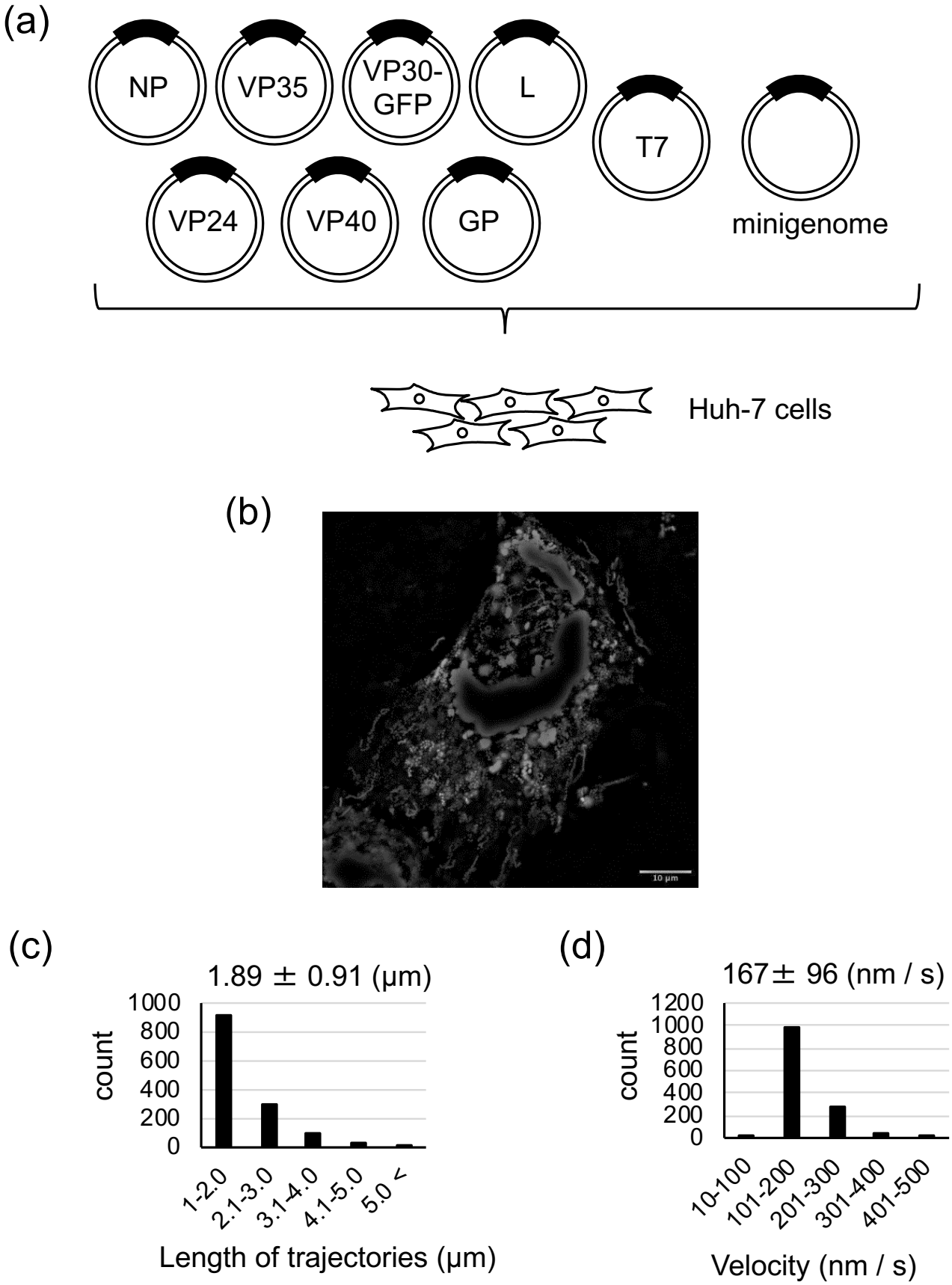
(a)
NP
VP35
VP30-GFP
L
T7
VP24
VP40
GP
minigenome
Huh-7 cells
(b)
10 μm
(c)
1.89 ± 0.91 (μm)
count
1000
800
600
400
200
0
1-2.0
2.1-3.0
3.1-4.0
4.1-5.0
5.0 <
Length of trajectories (μm)
(d)
167± 96 (nm / s)
count
1200
1000
800
600
400
200
0
10-100
101-200
201-300
301-400
401-500
Velocity (nm / s)

**Figure 2**

**Figure 3**

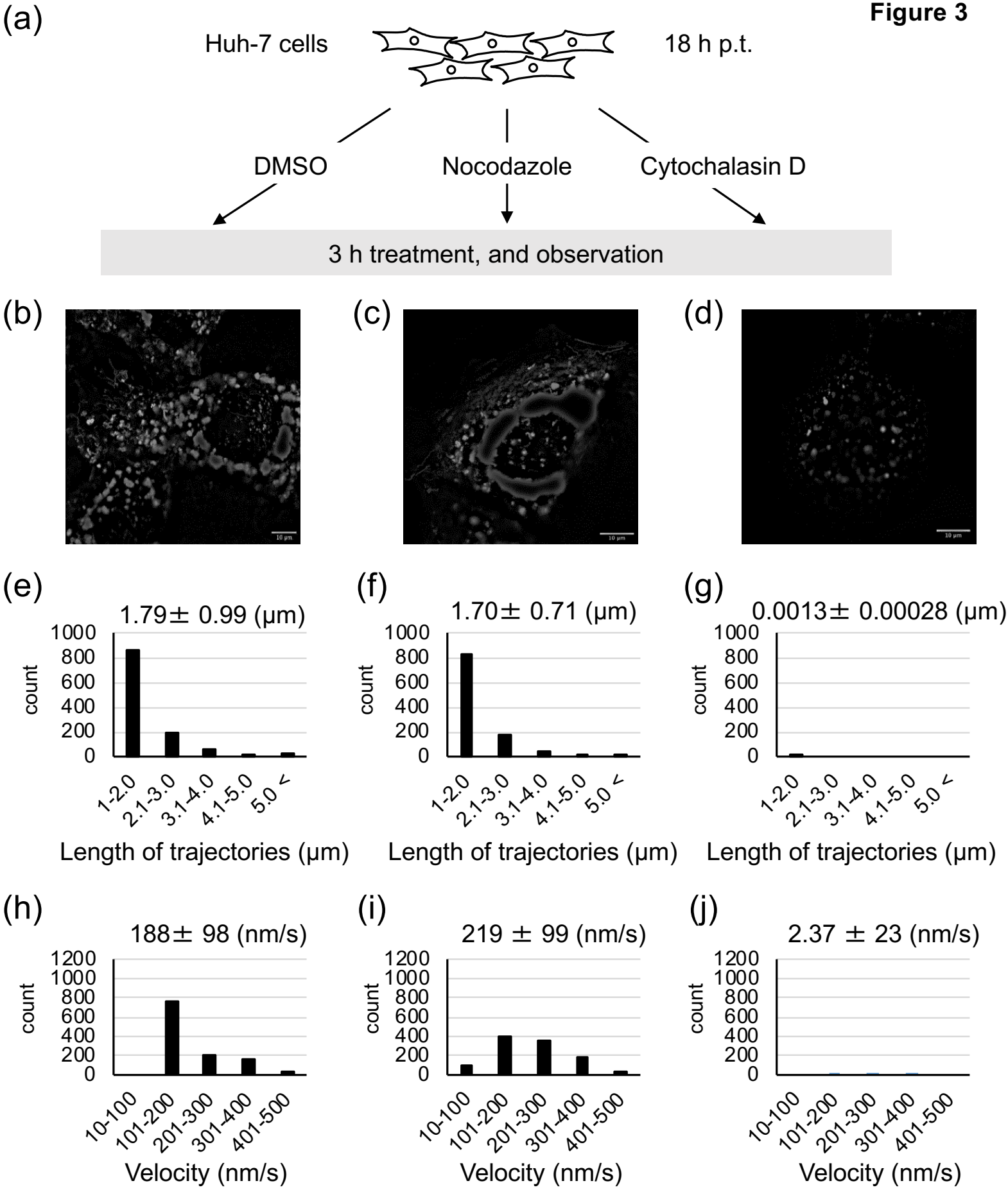
(a)
Huh-7 cells
18 h p.t.
DMSO
Nocodazole
Cytochalasin D
3 h treatment, and observation
(b)
(c)
(d)
(e)
1.79± 0.99 (μm)
count
1000
800
600
400
200
0
1-2.0
2.1-3.0
3.1-4.0
4.1-5.0
5.0 <
Length of trajectories (μm)
(f)
1.70± 0.71 (μm)
count
Length of trajectories (μm)
(g)
0.0013± 0.00028 (μm)
count
Length of trajectories (μm)
(h)
188± 98 (nm/s)
count
1200
1000
800
600
400
200
0
10-100
101-200
201-300
301-400
401-500
Velocity (nm/s)
(i)
219 ± 99 (nm/s)
count
Velocity (nm/s)
(j)
2.37 ± 23 (nm/s)
count
Velocity (nm/s)